5-9-2017

Spectroscopy and Formation of Lanthanum-Hydrocarbon Radicals Formed by C—C Bond Cleavage and Coupling of Propene

Dilrukshi C. Hewage
University of Kentucky, hewagedilrukshi@gmail.com

Wenjin Cao
University of Kentucky, wj.cao0707@uky.edu

Sudesh Kumari
University of Kentucky, sudeshchem@gmail.com

Ruchira Silva
University of Kentucky

Tao Hong Li
Southwest Forestry University, China

See next page for additional authors

Spectroscopy and formation of lanthanum-hydrocarbon radicals formed by C—C bond cleavage and coupling of propene

Dilrukshi Hewage,[1] Wenjin Cao,[1] Sudesh Kumari,[1] Ruchira Silva,[1] Tao Hong Li,[2] and Dong-Sheng Yang[1,a)]
[1]*Department of Chemistry, University of Kentucky, Lexington, Kentucky 40506-0055, USA*
[2]*Department of Chemistry, Southwest Forestry University, Kunming 650224, China*

(Received 16 February 2017; accepted 22 April 2017; published online 9 May 2017)

La reaction with propene is carried out in a laser-vaporization molecular beam source. Three La-hydrocarbon radicals are characterized by mass-analyzed threshold ionization (MATI) spectroscopy. One of these radicals is methylenelanthanum [La(CH_2)] (C_s), a Schrock-type metal carbene. The other two are a five-membered 1-lanthanacyclopent-3-en [La($CH_2CHCHCH_2$)] (C_s) and a tetrahedron-like trimethylenemethanelanthanum [La($C(CH_2)_3$)] (C_{3v}). Adiabatic ionization energies and metal-ligand stretching and hydrocarbon-based bending frequencies of these species are measured from the MATI spectra, preferred structures and electronic states are identified by comparing the experimental measurements and spectral simulations, and reaction pathways for the formation of the metal-hydrocarbon radicals are investigated with density functional theory calculations. All three radicals prefer doublet ground electronic states with La $6s^1$-based valence electron configurations, and singly charged cations favor singlet states generated by the removal of the La $6s^1$ electron. The metal-carbene radical is formed via multi-step carbon-carbon cleavage involving metallacyclization, β-hydrogen migration, and metal insertion. The metal-carbene radical formed in the primary reaction reacts with a second propene molecule to form the five-membered-ring and tetrahedron-like isomers through distinct carbon-carbon coupling paths. *Published by AIP Publishing.* [http://dx.doi.org/10.1063/1.4982949]

I. INTRODUCTION

Gas-phase studies of metal atom-mediated hydrocarbon activation provide an efficient means to investigate intrinsic reactivity patterns, reaction mechanisms, and structure-reactivity relationships without interferences from solvents and counterions. Such studies may also shed new insights on the single-metal atom catalysis.[1–5] Spectroscopic characterization of reactive intermediates in metal-mediated hydrocarbon activation reactions is desirable for better understanding how metal centers catalyze the C—H or C—C bond cleavage and functionalization. However, spectroscopy of transition metal-containing intermediates is challenging because these species are produced with a low number density and are of electronically open shells. Therefore, although a large body of thermodynamic and kinetic data is now available in the literature for gas-phase metal-hydrocarbon reactions as shown by numerous reviews,[6–16] spectroscopic measurements of metal-hydrocarbon species are lagged behind.[17–32]

As one of the simplest alkene molecules and the most important raw chemicals in petrochemical industry, metal-mediated propene activation has received considerable attentions.[6–10,14,15] For rare earth metal-propene reactions, previous studies have been reported on the product distributions and kinetics of both neutral atoms and positively charged ions. The Weisshaar group measured bimolecular rate constants, primary products, and kinetic isotope effects for the reaction of Y atoms in a fast flow reactor.[33] The primary products detected by time-of-flight (TOF) mass spectrometry were Y(C_3H_n) with product ratios of 8:48:44 for n = 2:4:6, and the product distributions showed no significant isotope effects. The Davis group examined the competition between C—C and C—H bond activation in crossed molecular beams.[34] The C—C bond cleavage led to the formation Y(CH_2) + C_2H_4, whereas the C—H cleavage yielded Y(C_3H_4) + H_2 and YH_2 + C_3H_4. The branching ratio of the C—C versus C—H cleavage (i.e., Y(CH_2)/Y(C_3H_4)) increased with the collision energy. Their experimental measurements and Rice-Ramsperger-Kassel-Marcus modeling indicated that all three channels involved the initial formation of π-association complexes, followed by Y inserting into one of the C—H bonds in the methyl group. The C—H cleavage products were formed by the decomposition of the inserted species through β—H migration, where the C—C bond activation involved the reverse β—H migration. The Schwarz group examined primary- and secondary-reaction products of Ce^+ and La^+ ions using Fourier-transform ion-cyclotron-resonance mass spectrometry.[35] The primary reactions led to the formation of $Ce(CH_2)^+$ and $Ce(C_3H_4)^+$, whereas the secondary reactions produced $Ce(C_nH_6)^+$ (n = 4 and 5) and $Ce(C_6H_m)^+$ (m = 6 and 8). La^+ reacted in almost the same manner as Ce^+, indicating that the Ce^+ 4f electron played no significant roles in such reactions. They proposed three possible isomers for $Ce(C_4H_6)^+$ based on the collision-induced dissociation (CID) measurements: Ce^+(butadiene), Ce^+(trimethylenemethane), and (methylene)Ce^+(allene).[35] Moreover, the reactivity trends

a)Author to whom correspondence should be addressed. Electronic mail: dyang0@uky.edu

of singly and doubly charged positive lanthanide ions with hydrocarbons, including propene, were investigated by several groups using mass-spectrometry based methods.[36–38] The general conclusions from those studies were that singly charged lanthanide ions with at least two non-f valence electrons (La^+, Ce^+, Gd^+, Pr^+, and Tb^+) in the ground or low-energy excited states and doubly charged ions with ground state or low-lying d^1 electron configurations (La^{2+}, Ce^{2+}, Gd^{2+}, and Tb^{2+}) were more reactive toward hydrocarbons than other lanthanides.

This work aims at the structural determinations of $La(CH_2)$ formed by the C—C bond cleavage and $La(C_4H_6)$ formed by the C—C coupling of propene using mass-analyzed threshold ionization (MATI) spectroscopy. By determining their structures, the formation of these species is investigated in combination with density functional theory (DFT) calculations. The work extends our recent study on the spectroscopic characterization of the La-mediated C—H bond activation of propene.[32] In that study, we identified spectroscopically an inserted species $HLa(\eta^3$-allyl) and two isomers of the dehydrogenated species $La(C_3H_4)$: lanthanacyclopropene and lanthanacyclobutene. The inserted species was formed by La inserting into an allylic C—H bond, the three-membered metallacycle by concerted vinylic H_2 elimination, and the four-membered ring by both allylic and vinylic dehydrogenation. To our knowledge, this is the first vibronic spectroscopic measurements of metal radicals formed by the C—C bond cleavage and coupling of propene.

This work is also a part of our recent efforts on La atom activations of small hydrocarbons.[28–32] La atom has a low-energy $5d^26s^1$ configuration that is able to minimize long range repulsive interactions and form two new chemical bonds with hydrocarbons. Because the electron promotion energy of La $5d^26s^1 \leftarrow 5d^16s^2$ (7.6 kcal mol^{-1}) is much smaller than those of Y ($4d^25s^1 \leftarrow 4d^15s^2$, 31.2 kcal mol^{-1}) or Sc ($3d^24s^1 \leftarrow 3d^14s^2$, 32.9.6 kcal mol^{-1})[39] atoms in the same group, La is expected to be more reactive toward small hydrocarbons than its lighter analogues. Moreover, La is essentially a monoisotopic element with 99.91% of ^{39}La, which simplifies the MATI spectroscopic experiment.

II. EXPERIMENTAL AND COMPUTATIONAL METHODS

The metal-cluster beam instrument used in this work consists of reaction and spectroscopy vacuum chambers and was described in a previous publication.[40] The metal-hydrocarbon reaction was carried out in a laser vaporization metal cluster beam source. Propene (99+ %, Aldrich) was seeded in a He carrier gas with a concentration of 10^{-4}-10^{-5} in a stainless steel mixing cylinder. La atoms were generated by pulsed-laser vaporization (Nd:YAG, Continuum Minilite II, 532 nm, 1.0-1.5 mJ/pulse) of a La rod (99.9%, Alfa Aesar) in the presence of the propene/carrier gas mixture (40 psi) delivered by a home-made piezoelectric pulsed valve. The metal atoms and gas mixture entered into a collision tube (2 mm diameter and 2 cm length) and were then expanded into the reaction chamber, collimated by a cone-shaped skimmer (2 mm inner diameter), and passed through a pair of deflection plates. Ionic species in the molecular beam that were formed during laser vaporization were removed by an electric field (100 V cm^{-1}) applied on the deflection plates. The neutral products were identified by photoionization TOF mass spectrometry. A separate experiment was carried out to confirm that propene was activated by La rather than the vaporization laser. In this experiment, propene was introduced by a second pulsed valve (Parker, Series 9) 3 cm downstream of the laser vaporization point. The reaction products formed in the two experiments were identical, though a higher propene concentration in the second experiment was required to produce comparable ion intensity in the mass spectra. Because propene bypassed the vaporization region in the second experiment, direct excitation of propene via the vaporization laser played no role in the hydrocarbon activation.

Prior to the MATI measurements, photoionization efficiency spectra of the La-hydrocarbon complexes were recorded to locate their approximate ionization thresholds to guide MATI scans. In the MATI experiment, each of the La complexes was excited to high-lying Rydberg states in a single-photon process and ionized by a delayed pulsed electric field. The excitation laser was the same as that for photoionization in the mass spectrometric and photoionization efficiency experiments and was the frequency doubled output of a tunable dye laser (Lumonics HD-500), pumped by the third harmonic output (355 nm) of a Nd:YAG laser (Continuum Surelite II). The laser beam was collinear and counter propagating with the molecular beam. The ionization pulsed field (320 V cm^{-1}) was generated by two high voltage pulse generators (DEI, PVX-4140) and delayed by 10-20 μs from the laser pulse by a delayed pulsed generator (SRS, DG645). A small dc field (6.0 V cm^{-1}) was used to separate the ions produced by direct photoionization from the MATI ions generated by delayed field ionization. The MATI ion signal was obtained by scanning the wavelength of the tunable dye laser, detected by a dual microchannel plate detector, amplified by a preamplifier (SRS, SR445), visualized by a digital oscilloscope (Tektronix TDS 3012), and stored in a laboratory computer. Laser wavelengths were calibrated against vanadium atomic transitions in the MATI spectral region after recording the MATI spectra for each species.[39] The Stark shift on the ionization energy (ΔIE) induced by the dc field (E_f) was calculated using the relation of $\Delta IE = 6.1E_f^{1/2}$, where E_f is in V cm^{-1} and ΔIE is in cm^{-1}.[41]

Geometry optimization and vibrational frequency calculations were carried out using Gaussian 09 software package.[42] In these calculations, we used the Becke's three-parameter hybrid functional with the correlation functional of Lee, Yang, and Parr (B3LYP), the 6-311+G(d,p) basis set for C and H, and the Stuttgart/Dresden (SDD) effective-core-potential basis set with 28 electron core for La atom.[43] We have extensively used DFT/B3LYP and found this method generally produced adequate results for the spectral and structural assignments of organometallic radicals.[27–30,44] No symmetry restrictions were imposed in initial geometry optimizations, but appropriate point groups were used in subsequent optimizations to identify electronic symmetries. For each optimized stationary point, a vibrational analysis was performed to identify the nature of the stationary point (minimum or saddle point). In predicting reaction pathways, minima connected by a

transition state were confirmed by intrinsic reaction coordinate calculations. In addition, potential energy scans were carried out to search for the transition state and energy minima of La(CH_2).

To compare with the experimental MATI spectra, multi-dimensional Franck-Condon (FC) factors were calculated from the equilibrium geometries, harmonic vibrational frequencies, and normal coordinates of the neutral and ionized complexes.[45] In these calculations, the recursion relations from Doktorov *et al.*[46] were employed, and the Duschinsky effect[47] was considered to account for a possible axis rotation from the neutral complex to the cation. Spectral simulations were obtained using the experimental line width and Lorentzian line shape. Transitions from excited vibrational levels of the neutral complex were considered by assuming thermal excitation at specific temperatures.

III. RESULTS AND DISCUSSION

A. MATI spectrum and structure of La(CH_2)

The MATI spectrum of La(CH_2) (Figure 1(a)) displays the strongest band at 42 265 (5) cm^{-1}, followed by a two-interval progression of 670 cm^{-1}, two weak transitions at 446 and 1258 cm^{-1}, and a combination band at 1116 (446 + 670) cm^{-1} (marked with "*"). The strong 42 265 cm^{-1} band is easily assigned as the origin band. Because of the short vibrational progression, the ejected electron by ionization is expected to be a non-bonding or weakly bound electron. This observation is similar to those of other La-hydrocarbon radicals formed by the C—H or C—C bond activation of other small hydrocarbons.[28–32] We will assign the spectral details after discussing the structure of the complex.

Although a MCH_2 (M = metal) complex may have multiple isomers such as (H_2)MC, HM(CH), or M(CH_2), previous theoretical calculations indicated that the most stable isomer is a M(CH_2) carbene species.[48–50] A CH_2 radical can be in triplet or singlet electronic states. The triplet state has one electron in a carbon sp^2 orbital and the other in a carbon p orbital, where the singlet state has the two electrons paired in a carbon sp^2 orbital. For transition metal atom interaction with a triplet methylene, a σ bonding occurs between the carbon sp^2 electron and a metal dσ electron, and a π bonding arises between the carbon p electron and a metal dπ electron. For metal interaction with a singlet methylene, the σ bonding is dative with the sp^2 electron lone-pair donation to an empty metal dσ orbital, whereas the π bonding is also dative but with a metal dπ electron pair back donation to an empty carbon p orbital. The metal carbene complex formed with the triplet methylene is called a Schrock carbene, whereas the complex formed with the singlet methylene is a Fisher carbene.[51] La atom has the ground electron configuration $5d^16s^2$, which is not suitable for bonding with either the triplet or singlet carbene because there is only one d electron. For La to bind with CH_2, a 5d ← 6s electron promotion is thus required. The lowest-energy state with a $5d^26s^1$ electron configuration is a ^4F state at 2668 cm^{-1}. The La ^4F ($5d^26s^1$) state is appropriate for binding with the triplet CH_2 to form a Schrock carbene complex, where each of the two unpaired La 5d electrons is spin paired with a carbon p or sp^2 electron in a bonding combination to form two La—C covalent bonds. Each of the resultant La—C bonds is polarized toward C because C is more electronegative than La, leading to a net negative charge on the C atom. The ground state of the resultant Schrock carbene is thus expected to be a doublet with a La-valence $6s^1$ electron configuration.

To quantify the above qualitative arguments, we carried out DFT/B3LYP calculations on the neutral and ion states of La(CH_2). The structure of the neutral doublet ($^2A'$) is shown as an energy minimum in Figure 2. The electron configuration of the doublet is La $6s^1$ as expected, and the complex is in a planar C_s symmetry. The structure of La(CH_2) is featured with a La=C double bond (2.090 Å), slightly unequal C—H bonds (1.092 Å vs 1.122 Å), and very different La—C—H bond angles (90.5° vs 158.2°). The metal-carbon bond has largely a double-bond character because it is much shorter than the La—C single bonds in La(C_2H_2) (2.306 Å).[29,30] The unequal C—H bond lengths and La—C—H bond angles are a bit surprising at the first glance, but similar structural features have been observed in the solution phase[52,53] and predicted in the gas phase.[49,50,54] The unequal C—H bond lengths and La—C—H bond angles are due to a so-called agostic interaction, that is, a three-center-two-electron interaction involving a La—H—C group.[53] In this type of interactions, the bonding electrons of a C—H σ bond are donated to the metal center to

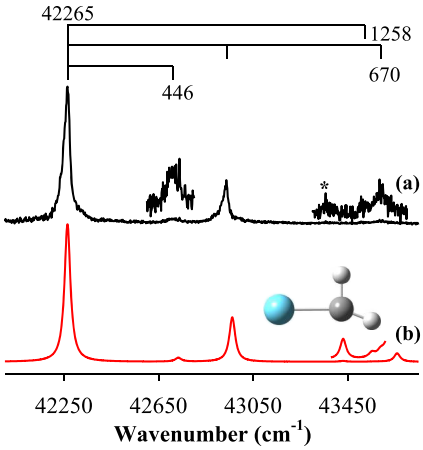

FIG. 1. MATI spectrum of La(CH_2) (a) and simulation of the $^1A' \leftarrow {}^2A'$ transition of the La(CH_2) (C_s) complex at 200 K (b). "*" donates a combination band.

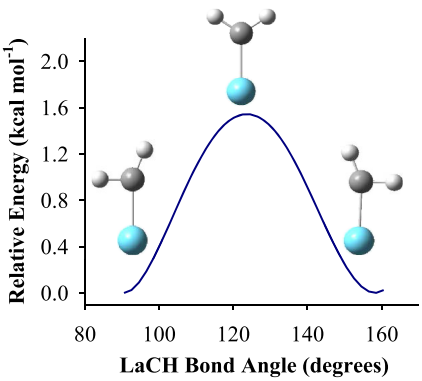

FIG. 2. Potential energy scan of La(CH_2) as a function of a La—C—H bond angle calculated at the DFT/B3LYP level.

form a three-center-two-electron bond. If the metal center is electron rich, a back donation could also occur from the metal center to the antibonding σ* orbital of the C—H bond. If the back donation is sufficiently strong, the C—H bond may be broken due to the electron occupation in the σ* orbital. However, La atom in the Schrock carbene is electron deficient, and the back electron donation is not efficient. Because of the weak back donation, the C—H bond that participates in the agostic interaction is only slightly weaker than the other C—H bond as demonstrated by the slightly longer bond length (by 0.030 Å) predicted by the DFT calculations. The removal of the La $6s^1$ electron by ionization leads to a singlet ion state ($^1A'$) with a very similar geometry to that of the neutral doublet state ($^2A'$). The small change in the structure upon ionization is consistent with the qualitative arguments and computational prediction of the non-bonding La $6s^1$ electron in the highest occupied orbital. The somewhat shorter La=C distance in the ion than in the neutral state (by 0.052 Å) arises from the enhanced charge-multipole interactions.

Because an isolated La atom has three valence electrons, we have also searched for a quartet neutral state. The quartet state was, however, predicted to be about 1 eV higher than the doublet state with a La—C single bond (2.417 Å). Because of its high energy, this state will not be discussed further. Because previous high-level *ab initio* calculations predicted the $La(CH_2)^+$ to be in a more symmetric C_{2v} structure,[48,49] we have also carried out geometry optimization under a C_{2v} symmetry constraint. However, the optimized C_{2v} structure ($^2A_1$) has an imaginary frequency associated with a H rocking motion. Thus, the C_{2v} structure is a transition state, not an energy minimum. Figure 2 presents a potential energy scan of $La(CH_2)$ as a function of a La—C—H bond angle. As demonstrated by the figure, the potential energy increases first as the bond angle increases from 90° to 125° and then decreases as it increases from 125° to 158°. The energy barrier from C_s to C_{2v} is predicted to be ~1.5 kcal mol^{-1}.

Figure 1(b) shows the spectral simulation of the $^1A' \leftarrow {}^2A'$ transition of La (CH_2) (C_s) at 200 K. In this simulation, the calculated 0–0 transition energy (43 064 cm^{-1}) of $La(CH_2)$ is aligned with the 42 265 cm^{-1} origin band, but the calculated vibrational frequencies are unscaled in order to directly compare with the measured spectrum. The simulation nicely reproduces the measured 670 cm^{-1} progression and 446, 1116, and 1258 cm^{-1} weak bands. The calculated frequencies for these transitions are 697, 467, 1164, and 1324 cm^{-1}, which are in reasonable agreement with the experimental values. The 670 cm^{-1} progression and the 446 cm^{-1} band are assigned to the vibronic transitions from the zero vibrational level of the $^2A'$ neutral state to the La—C stretching (ν_4^+, a′) and CH_2 rocking (ν_5^+, a′) motions of the $^1A'$ ion state, respectively; the 1116 cm^{-1} band is the combination band of the metal-ligand stretching and CH_2 rocking excitations, and the 1258 cm^{-1} band is due to a CH_2 scissoring excitation (ν_3^+, a′) in the ion state. Previously, the dissociation energies (D_0^+) of the $La^+—CH_2$ bond were measured to be 4.26 ± 0.06 eV with ion beam mass spectrometry[55] and 4.6 ± 0.2 with photoionization measurements.[56] If $D_0^+(La^+—CH_2)$ = 4.26 ± 0.06 eV is used in the thermodynamic relation, we obtain $D_0(La—CH_2)$ = 3.92 ± 0.06 eV by involving adiabatic ionization energy (AIE) (La) = 5.5769 eV[57] and AIE [$La(CH_2)$] = 5.240 ± 0.001 eV.

B. MATI spectrum and two isomers of $La(C_4H_6)$

The MATI spectrum of $La(C_4H_6)$ displays two band systems (Figures 3(a) and 3(b)). The first system originates at 39 418 (5) cm^{-1}. To the blue of the origin band, it shows a two-quantum 396 cm^{-1} progression, 470 and 318 cm^{-1} intervals, 714 (396 + 318) (marked with "*1") and 866 (396 + 470) cm^{-1} (marked with "*2") combination bands, and 22 cm^{-1} satellite bands superimposed on the 396 cm^{-1} progression. To the red, 374 and 289 cm^{-1} weak bands are also observed. The second band systems exhibit the origin band at 41 264 (5) cm^{-1}; a strong three-quantum 353 cm^{-1} progression, a weak two-quantum 240 cm^{-1} progression, and three other weak bands at 572 (marked with "#"), 900, and 958 cm^{-1} above the origin band; and a weak 326 cm^{-1} band below.

Previously, the Schwarz group proposed three possible isomers for $Ce^+(C_4H_6)$ formed by the Ce^+ + propene reaction: Ce^+(butadiene), Ce^+(trimethylenemethane), and (methylene)Ce^+(allene).[35] To try to pinpoint which isomer(s) was/were produced by the Ce^+ + propene reaction, they performed CID measurements of $Ce^+(C_4H_6)$ generated by Ce^+ reactions with five different hydrocarbons (i.e., propene, n-butane, isobutane, 1-butene, and isobutene) and proposed Ce^+(butadiene) to be the most likely isomer for the reaction with propene. However, because of different internal energies of the metal ions produced from the hydrocarbon reactions and possible rearrangements upon collisions of kinetically excited ions with the target gas, a precise interpretation of the CID spectra may not be straightforward. In our computational search for the isomer(s) of $La(C_4H_6)$ from the La + propene reaction, we considered all three possible isomers proposed by the Schwarz group and located four energy minima as shown in Figure 4. The most stable isomer is predicted to be trimethylenemethanelanthanum [$La(C(CH_2)_3)$] (C_{3v}), followed by 1-lanthanacyclopent-3-ene (C_s) [$La(CH_2CHCHCH_2)$] at

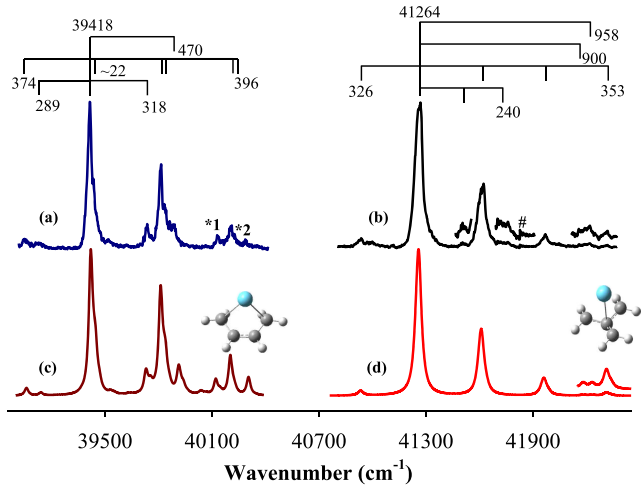

FIG. 3. MATI spectrum of $La(C_4H_6)$ in two spectral regions ((a) and (b)) and simulations (200 K) of the $^1A' \leftarrow {}^2A'$ transition of 1-lanthanacyclopent-3-ene [$La(CH_2CHCHCH_2)$] (C_s) (c) and the $^1A_1 \leftarrow {}^2A_1$ transition of the trimethylenemethanelanthanum [$La(C(CH_2)_3)$] (C_{3v}) (d). "*1" and "*2" are combination bands, and "#" is a band not clearly shown in the simulation.

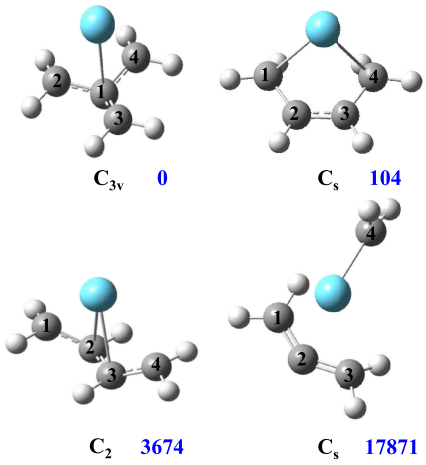

FIG. 4. Four isomers of La(C_4H_6) with point groups and relative energies (cm^{-1}) computed at the DFT/B3LYP level.

104 cm^{-1}, (*trans*-butadiene)lanthanum [La(*trans*-C_4H_6)] (C_2) at 3674 cm^{-1}, and (methylene)La(allene) [(CH_2)La(C_3H_4)] (C_s) at 17 871 cm^{-1}. The ground states of these isomers are doublets with quartet states at ≥8000 cm^{-1}. Four minimum-energy isomers, instead of three, are located because a butadiene molecule has *cis* and *trans* conformations. La binding with the *cis*- and *trans*-forms yields 1-metallacyclopent-3-ene and (*trans*-butadiene)lanthanum, respectively. Because the MATI spectrum exhibits only two band systems, the doublet ground states of the two lowest-energy isomers are probably the spectral carriers as discussed below.

Figures 3(c) and 3(d) show the spectral simulations (200 K) of the $^1A' \leftarrow {}^2A'$ transition of La($CH_2CHCHCH_2$) (C_s) and the $^1A_1 \leftarrow {}^2A_1$ transition of La($C(CH_2)_3$) (C_{3v}). As in the case of La(CH_2), the calculated the AIEs of the two isomers are aligned with energies of the two origin bands, but the predicted vibrational frequencies are unscaled. The simulation of the $^1A' \leftarrow {}^2A'$ transition of La($CH_2CHCHCH_2$) is in excellent agreement with the lower-energy band system (Table I and Figures 3(a) and 3(c)). On the basis of the spectral simulation, the observed 470, 396, and 318 cm^{-1} intervals are assigned to excitations of a symmetric La-ligand stretch coupled with a terminal CH_2 rock (ν_{11}^+, a′), a second symmetric La-ligand stretch mixed with another terminal CH_2 rock (ν_{12}^+, a′), and a symmetric C—H bend of the middle HCCH group of H_2C—HC=CH—CH_2 (ν_{13}^+, a′) in the $^1A'$ ion state; 374 and 289 cm^{-1} intervals to the second La-ligand stretch/CH_2 rock (ν_{12}, a′) and C—H bend excitations (ν_{13}, a′) in the $^2A'$ neutral state; and the 22 cm^{-1} satellite bands to sequence transitions of a symmetric C—La—C bending mode (ν_{14}^+ -ν_{14}). The major difference between the two La-ligand stretch/CH_2 rock modes (ν_{11}^+ and ν_{12}^+) is the opposite directions of the CH_2 rocking motions. These assignments are consistent with those of the previously observed La(C_4H_6) formed in the reaction of La with ethylene.[30]

The simulation of the $^1A_1 \leftarrow {}^2A_1$ transition of La($C(CH_2)_3$) (C_{3v}) reproduces the measured 353 cm^{-1} progression, the 326 cm^{-1} transition below the origin band, and even the very weak transitions at 900 and 958 cm^{-1} above the origin band. The 353/326 cm^{-1} intervals are attributed to the symmetric La-ligand stretching excitations (ν_6^+/ν_6, a_1) of the $^1A_1$ ion/$^2A_1$ neutral states, and the weak 900 and 958 cm^{-1} transitions to the CH_2 wag (ν_4^+, a_1) and $C(CH_2)_3$ deformation (ν_3^+, a_1) in the ion, respectively. The calculated frequencies for these observed modes are 351/327, 924, and 975 cm^{-1}, which again are in reasonable agreement with the experimental values. The predicted AIE for this isomer, 41 810 cm^{-1}, is also in very good agreement with the measured value 41 264 cm^{-1}. The

TABLE I. AIEs (cm^{-1}) and vibrational frequencies (cm^{-1}) of the La(CH_2) (C_s), 1-lanthanacyclopent-3-ene [La($CH_2CHCHCH_2$)] (C_s), and trimethylenemethanelanthanum [La($C(CH_2)_3$)] (C_{3v}) complexes from MATI spectroscopy and DFT/B3LYP calculations.

Complexes	MATI	B3LYP	Mode description
		La(CH_2) (C_s), ($^1A' \leftarrow {}^2A'$)	
AIE	42 265	43 142	
ν_3^+, a′	1 258	1 324	CH_2 scissor
ν_4^+, a′	670	697	La—C stretch
ν_5^+, a′	446	469	CH_2 rock
		La($CH_2CHCHCH_2$) (C_s), ($^1A' \leftarrow {}^2A'$)	
AIE	39 418	40 164	
ν_{11}^+, a′	470	492	Terminal CH_2 rock and symmetric La-ligand stretch
ν_{12}^+/ν_{12}, a′	396/374	391/359	Symmetric La-ligand stretch and terminal CH_2 rock
ν_{13}^+/ν_{13}, a′	318/289	309/279	C—H bend of middle CH_2 group
ν_{14}^+/ν_{14}, a′		217/192	Symmetric C—La—C bend
$\nu_{14}^+ - \nu_{14}$	22	25	
		La($C(CH_2)_3$) (C_{3v}), ($^1A_1 \leftarrow {}^2A_1$)	
AIE	41 264	41 810	
ν_3^+, a_1	958	975	$C(CH_2)_3$ deformation
ν_4^+, a_1	900	924	CH_2 wag
ν_6^+/ν_6, a_1	353/326	351/327	Symmetric La-ligand stretch
ν_9^+, a_2	572	575	CH_2 twist
ν_{18}^+, e	240	234	Asymmetric La-ligand stretch

agreements between the theory and experiment indicate that assigning the La(C(CH$_2$)$_3$) isomer as the carrier of the second band system is reasonable. However, the simulation fails to reproduce the weak 240 cm^{-1} progression and 572 cm^{-1} band. The only harmonic modes close to the measured intervals are a doubly degenerate e mode of 230 cm^{-1} and a non-degenerate a_2 mode of 575 cm^{-1}. Both e and a_2 modes are not supposed to be active based on the first-order selection rule. Reasons for the discrepancy are not certain but may be discussed as follows. First, the complex could have a lower-symmetry structure. To investigate this possibility, we carried out additional geometry optimizations with the initial guesses of C_s and C_1 structures. However, both the C_s and C_1 initial guesses were converged to C_{3v} symmetry. Second, the activity of the e and a_2 modes could be due to the Herzberg-Teller effect.[58] The Herzberg-Teller effect may involve non-totally symmetric vibrations in an allowed electronic transition (as in the current case) and lead to the intensity stealing of a non-totally symmetric mode from other electronic transitions. For example, the vibronic species with one quantum excitation of an e mode in the $^1A_1$ ion state is $^1E^{ev}$, where the superscript "ev" stands for a vibronic state. The $^1E^{ev}$ vibronic state is then coupled to a nearby electronic state of the same symmetry (i.e., ^1E), resulting in the intensity being stolen by the vibronic transition ($^1E^{ev} \leftarrow {}^2A_1$) from the allowed electronic transition ($^1E \leftarrow {}^2A_1$). For the $^1A_1$ ion state, the electron configuration is $a_1{}^2e^4a_1{}^0$. Excitation of an electron from the highest occupied molecular orbital (HOMO, e^4) to the lowest unoccupied molecular orbital (LUMO, a_1) yields an excited electron configuration $a_1{}^2e^3a_1{}^1$. Electronic states associated with $a_1{}^2e^3a_1{}^1$ are $^{1,3}E$. The strength of the $^1E^{ev}$ and ^1E coupling depends on the energy difference between the two states, which is estimated to be ~3.5 eV using E(LUMO) – E(HOMO) of the $^1A_1$ state. Because the $^1E^{ev}$ and ^1E states are quite apart in energy, their coupling is expected to be weak. A third possibility is the failure of the harmonic approximation. To investigate this possibility, we calculated anharmonic frequencies of the La(C(CH$_2$)$_3$)$^+$ $^1A_1$ ion at the same level of theory as that used for the harmonic frequency calculations. Such calculations produced the anharmonic frequencies of $-336i$ and 69 cm^{-1} for the e_2 mode (versus the harmonic frequencies of 234 cm^{-1}) and 260 cm^{-1} for the a_2 mode (versus the harmonic frequency of 575 cm^{-1}). Although these calculations may suggest a considerable anharmonicity of the two modes, the predicted imaginary or very small anharmonic frequencies cause some doubts about the reliability of the anharmonic calculations as previously reported for metal-aniline radicals.[59]

C. Formation of La(CH$_2$), La(CH$_2$CHCHCH$_2$), and La(C(CH$_2$)$_3$)

Figure 5 presents the potential energy profile along the reaction coordinates for the formation of methylenelanthanum La(CH$_2$), a Schrock-type metal carbene complex. The first step is the exothermic formation of a metallacyclopropene (IM1). The second step involves La insertion into a methyl C—H bond to form an inserted intermediate (IM2) via transition state TS1. La prefers the insertion of a methyl C(sp^3)—H bond rather than a vinylic C(sp^2)—H bond because the former is weaker than the latter.[57] The next step engages a H migration from La to the

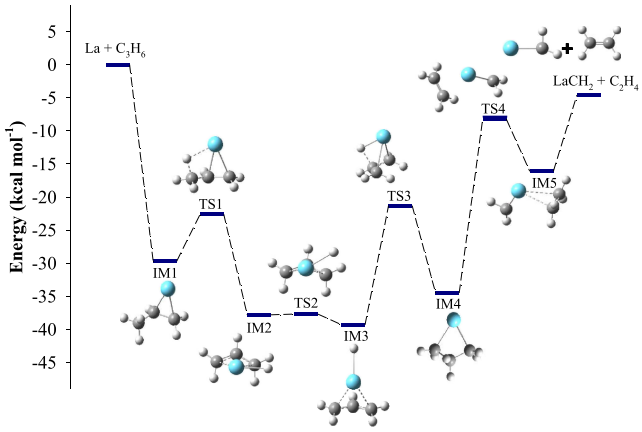

FIG. 5. Reaction pathway and energy profile for the formation of La(CH$_2$)(C_s) from the La + propene reaction calculated at the DFT/B3LYP level. IMn stands for intermediates and TSn transition states.

middle carbon atom to form a metallacyclobutane (IM4) via TS2, IM3, and TS3. IM3 is different from the previously identified inserted structure of HLa(η^3-allyl), with the La-bound H atoms of the two species in nearly opposite orientations.[32] The above-mentioned three steps from IM1 to IM4 complete a H migration process from the methyl sp^3 carbon to a vinylic sp^2 carbon (i.e., β—H migration). Because a vinylic C—H bond is stronger than an allylic C—H bond, IM4 is more stable than IM1. The final step is associated with La insertion into a C(sp^3)—C(sp^3) bond to form (CH$_2$)La(C$_2$H$_4$) (IM5) through TS4, which is then decomposed into La(CH$_2$) + C$_2$H$_4$. The whole process is barrierless and exothermic by 4.6 kcal mol^{-1} with vibrational zero point corrections. In addition to the aforementioned pathway, La(CH$_2$) could also been formed by La inserting into the C(sp^2)—C(sp^3) or C(sp^2)—C(sp^2) bond, but either of these two pathways is expected to be thermodynamically less favorable as previously reported for the reaction of Y + propene.[34,60]

The metal carbene radical reacts further with a second propene molecule to form 1-lanthanacyclopent-3-ene [La(CH$_2$CHCHCH$_2$)] and trimethylenemethanelanthanum La[C(CH$_2$)$_3$] as shown in Figure 6. The first step for both isomers is the formation of an entrance channel π complex (IM6) between La(CH$_2$) and propene, where the C=C double bond of the alkene remains intact. From IM6, the formation of the two isomers takes different paths. In the case of La(CH$_2$CHCHCH$_2$), the second step involves the formation of a four-membered metallacycle intermediate (IM7) through the coupling of the carbon atom of the metal carbene and the terminal vinylic carbon of propene and the binding of La with the middle vinylic carbon of propene. In this metallacycle, all carbon atoms become sp^3 hybridized. The third step includes La inserting into a C—H bond of the middle CH$_2$ group (IM8), followed by a rotation of the metal-bound H atom to yield IM9 and IM10 and a second La insertion into a C—H bond of the methyl group (IM11). The final step is a concerted H$_2$ elimination to produce La(CH$_2$CHCHCH$_2$) + H$_2$. In the case of La(C(CH$_2$)$_3$), the second step includes a CH$_2$ rotation (IM12), followed by the carbene carbon coupling with the middle carbon of propene (IM13). The third step implicates sequential La insertions into the C—H bond of the

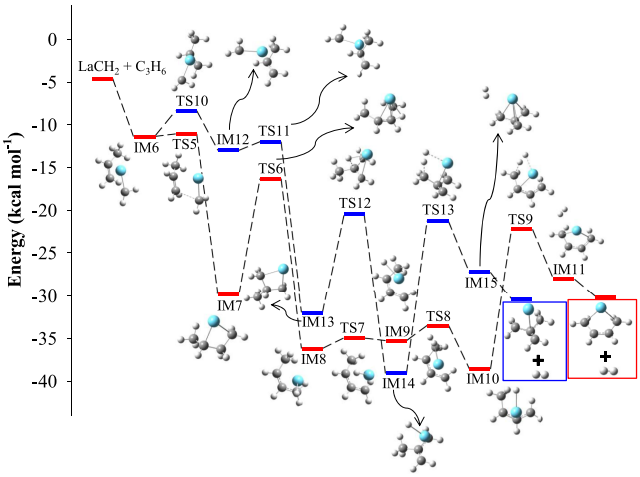

FIG. 6. Reaction pathways and energy profiles for the formation of $La(CH_2CHCHCH_2)$ (C_s) and $La[C(CH_2)_3]$ (C_{3v}) from the La + propene reaction calculated at the DFT/B3LYP level. IMn stands for intermediates and TSn transition states. The energies are relative to that of La + 2 C_3H_6, but C_2H_4 from a primary reaction is not included in order to simplify the figure.

μ_3-methanetriyl group (IM14) and a C—H bond of the methyl group (IM15). Similar to $La(CH_2CHCHCH_2)$, $La(C(CH_2)_3)$ is then formed by a concerted H_2 elimination process. These processes have no overall energy barriers and are exothermic by 25.5 kcal mol^{-1} for the formation of $La(CH_2CHCHCH_2)$ and 25.9 kcal mol^{-1} for $La(C(CH_2)_3)$ with respect to $LaCH_2 + C_3H_6$.

IV. CONCLUSIONS

We have reported the MATI spectroscopic characterization of $La(CH_2)$ and two isomers of $La(C_4H_6)$ radicals formed by the C—C bond activation of propene. $La(CH_2)$ is identified as methylenelanthanum, a Schrock-type metal-carbene species involving a three-center two-electron agostic interaction. Two isomers of $La(C_4H_6)$ are observed to be 1-lanthanacyclopent-3-en [$La(CH_2CHCHCH_2)$] and methylenemethanelanthanum [$La(C(CH_2)_3)$]. The spectroscopic measurements yield adiabatic ionization energies and metal-ligand stretching and ligand-based bending frequencies for all three species. The ground state of each radical is a doublet with a La-based $6s^1$ electron configuration and that of the corresponding ion is a singlet. Because of the non-bonding nature of the La $6s^1$ electron, ionization has a very small effect on the geometry of the neutral state. The formation of the metal-carbene radical involves metallacyclization, β—H migration, metal insertion into a C—C bond, and C—C bond cleavage. The metal-carbene intermediate reacts with a second propene molecule to form the two $La(C_4H_6)$ isomers via different carbon-carbon coupling and dehydrogenation paths.

SUPPLEMENTARY MATERIAL

See the supplementary material for the geometries of $La(CH_2)$, $La(CH_2CHCHCH_2)$ and $La(C(CH_2)_3)$, and their ion states; energies of the stationary points along the reaction coordinates for the formation of three La-hydrocarbon radicals.

ACKNOWLEDGMENTS

We are grateful for the financial support from the National Science Foundation Division of Chemistry (Chemical Structure, Dynamics, and Mechanisms, Grant No. CHE-1362102). We also acknowledge additional support from the Kentucky Science and Engineering Foundation.

[1] B. Qiao, A. Wang, X. Yang, L. F. Allard, Z. Jiang, Y. Cui, J. Liu, J. Li, and T. Zhang, Nat. Chem. **3**, 634 (2011).
[2] G. Kyriakou, M. B. Boucher, A. D. Jewell, E. A. Lewis, T. J. Lawton, A. E. Baber, H. L. Tierney, M. Flytzani-Stephanopoulos, and E. C. Sykes, Science **335**, 1209 (2012).
[3] A. Figueroba, G. Kovacs, A. Bruix, and K. M. Neyman, Catal. Sci. Technol. **6**, 6806 (2016).
[4] J. Jones, H. Xiong, A. T. DeLaRiva, E. J. Peterson, H. Pham, S. R. Challa, G. Qi, S. Oh, M. H. Wiebenga, X. I. Pereira Hernandez, Y. Wang, and A. K. Datye, Science **353**, 150 (2016).
[5] W. Liu, L. X. Zhang, W. Yan, X. Liu, X. Yang, S. Miao, W. Wang, A. Wang, and T. Zhang, Chem. Sci. **7**, 5758 (2016).
[6] K. Eller and H. Schwarz, Chem. Rev. **91**, 1121 (1991).
[7] J. C. Weisshaar, Acc. Chem. Res. **26**, 213 (1993).
[8] *Organometallic Ion Chemistry*, edited by B. S. Freiser (Kluwer, Dordrecht, 1996).
[9] J. J. Schroden and H. F. Davis, in *Modern Trend in Chemical Dynamics Part II: Experiment and Theory*, Advanced Series in Physical Chemistry, edited by X. Yang and K. Lium (World Scientific, Singapore, 2004), Vol. 14, p. 215.
[10] D. K. Bohme and H. Schwarz, Angew. Chem., Int. Ed. **44**, 2336 (2005).
[11] J. Roithova and D. Schroeder, Chem. Rev. **110**, 1170 (2010).
[12] H. Schwarz, Angew. Chem., Int. Ed. **50**, 10096 (2011).
[13] P. B. Armentrout, Catal. Sci. Technol. **4**, 2741 (2015).
[14] P. B. Armentrout, Int. J. Mass Spectrom. **377**, 54 (2015).
[15] M. T. Rodgers and P. B. Armentrout, Chem. Rev. **116**, 5642 (2016).
[16] S. Zhou, J. Li, M. Schlangen, and H. Schwarz, Acc. Chem. Res. **49**, 494 (2016).
[17] R. S. Walters, E. D. Pillai, P. v. R. Schleyer, and M. A. Duncan, J. Am. Chem. Soc. **127**, 17030 (2005).
[18] A. D. Brathwaite, T. B. Ward, R. S. Walters, and M. A. Duncan, J. Phys. Chem. A **119**, 5658 (2015).
[19] S. R. Miller, T. P. Marcy, E. L. Millam, and D. G. Leopold, J. Am. Chem. Soc. **129**, 3482 (2007).
[20] M. A. Ashraf, C. W. Copeland, A. Kocak, A. R. McEnroe, and R. B. Metz, Phys. Chem. Chem. Phys. **17**, 25700 (2015).
[21] A. Kocak, M. A. Ashraf, and R. B. Metz, J. Phys. Chem. A **119**, 9653 (2015).
[22] V. J. F. Lapoutre, B. Redlich, A. F. G. van der Meer, J. Oomens, J. M. Bakker, A. Sweeney, A. Mookherjee, and P. B. Armentrout, J. Phys. Chem. A **117**, 4115 (2013).
[23] O. W. Wheeler, M. Salem, A. Gao, J. M. Bakker, and P. B. Armentrout, J. Phys. Chem. A **120**, 6216 (2016).
[24] M. A. Flory, A. J. Apponi, L. N. Zack, and L. M. Ziurys, J. Am. Chem. Soc. **132**, 17186 (2010).
[25] D. J. Brugh and M. D. Morse, J. Chem. Phys. **141**, 064304 (2014).
[26] M. A. Garcia and M. D. Morse, J. Phys. Chem. A **117**, 9860 (2013).
[27] Y. Zhang, M. W. Schmidt, S. Kumari, M. S. Gordon, and D.-S. Yang, J. Phys. Chem. A **120**, 6963 (2016).
[28] D. Hewage, M. Roudjane, W. R. Silva, S. Kumari, and D.-S. Yang, J. Phys. Chem. A **119**, 2857 (2015).
[29] D. Hewage, W. R. Silva, W. Cao, and D.-S. Yang, J. Am. Chem. Soc. **138**, 2468 (2016).
[30] S. Kumari, W. Cao, Y. Zhang, M. Roudjane, and D.-S. Yang, J. Phys. Chem. A **120**, 4482 (2016).
[31] D. Hewage, W. Cao, J. H. Kim, Y. Wang, Y. Liu, and D.-S. Yang, J. Phys. Chem. A **121**, 1233 (2017).
[32] S. Kumari, W. Cao, D. Hewage, R. Silva, and D.-S. Yang, J. Chem. Phys. **146**, 074305 (2017).
[33] M. Porembski and J. C. Weisshaar, J. Phys. Chem. A **105**, 6655 (2001).
[34] R. Z. Hinrichs, J. J. Schroden, and H. F. Davis, J. Phys. Chem. A **107**, 9284 (2003).
[35] C. Heinemann, D. Schroeder, and H. Schwarz, Chem. Ber. **127**, 1807 (1994).
[36] J. B. Schilling and J. L. Beauchamp, J. Am. Chem. Soc. **110**, 15 (1988).
[37] H. H. Cornehl, C. Heinemann, D. Schroeder, and H. Schwarz, Organometallics **14**, 992 (1995).

[38]J. Marcalo, M. Santos, A. P. de Matos, J. K. Gibson, and R. G. Haire, J. Phys. Chem. A **112**, 12647 (2008).
[39]C. E. Moore, *Atomic Energy Levels* (National Bureau of Standards, Washington, DC, 1971).
[40]B. R. Sohnlein, S. G. Li, J. F. Fuller, and D.-S. Yang, J. Chem. Phys. **123**, 014318 (2005).
[41]M. A. Duncan, T. G. Dietz, and R. E. Smalley, J. Chem. Phys. **75**, 2118 (1981).
[42]M. J. Frish, G. W. Trucks, H. B. Schlegel, G. E. Scuseria, M. A. Robb, J. R. Cheeseman, G. Scalmani, V. Barone, B. Mennucci, G. A. Petersson, H. Nakatsuji, M. Caricato, X. Li, H. P. Hratchian, A. F. Izmaylov, J. Bloino, and G. Zheng, GAUSSIAN 09, Revision A.01, Gaussian, Inc., Wallingford, CT, 2009.
[43]M. Dolg, H. Stoll, A. Savin, and H. Preuss, Theor. Chim. Acta **75**, 173 (1989).
[44]D.-S. Yang, J. Phys. Chem. Lett. **2**, 25 (2011).
[45]S. Li, "Threshold photoionization and ZEKE photoelectron spectroscopy of metal complexes," Ph.D. thesis, University of Kentucky, 2004.
[46]E. V. Doktorov, I. A. Malkin, and V. I. Man'ko, J. Mol. Spectrosc. **64**, 302 (1977).
[47]F. Duschinsky, Acta Physicochim. **7**, 551 (1937).
[48]K. K. Irikura and W. A. Goddard, J. Am. Chem. Soc. **116**, 8733 (1994).
[49]B. O. Roos and P. Pyykko, Chem. - Eur. J. **16**, 270 (2010).
[50]L. G. M. de Macedo and P. Pyykkoe, Chem. Phys. Lett. **462**, 138 (2008).
[51]R. H. Crabtree, *The Organometallic Chemistry of the Transition Metals*, 3rd ed. (Wiley, New Haven, Connecticut, 2001).
[52]R. J. Goddard, R. Hoffmann, and E. D. Jemmis, J. Am. Chem. Soc. **102**, 7667 (1980).
[53]M. Brookhart, M. L. H. Green, and G. Parkin, Proc. Natl. Acad. Sci. U. S. A. **104**, 6908 (2007).
[54]R. M. Cox, P. B. Armentrout, and W. A. de Jong, Inorg. Chem. **54**, 3584 (2015).
[55]L. S. Sunderlin and P. B. Armentrout, J. Am. Chem. Soc. **111**, 3845 (1989).
[56]R. L. Hettich and B. S. Freiser, J. Am. Chem. Soc. **109**, 3543 (1987).
[57]D. R. Lide, *CRC Handbook of Chemistry and Physics*, 88th ed. (CRC, Boca Raton, FL, 2008).
[58]J. M. Hollas, *High Resolution Spectroscopy*, 2nd ed. (Wiley, New York, 1998).
[59]S. Kumari, B. Sohnlein, D. Hewage, M. Roudjane, J. Lee, and D.-S. Yang, J. Chem. Phys. **138**, 224304 (2013).
[60]T. H. Li and X. G. Xie, J. Phys. Org. Chem. **23**, 768 (2010).

Spectroscopy and formation of lanthanum-hydrocarbon radicals formed by C—C bond cleavage and coupling of propene

Dilrukshi Hewage, Wenjin Cao, Sudesh Kumari, Ruchira Silva, Tao Hong Li, and Dong-Sheng Yang

Citation: The Journal of Chemical Physics **146**, 184304 (2017); doi: 10.1063/1.4982949
View online: https://doi.org/10.1063/1.4982949
View Table of Contents: http://aip.scitation.org/toc/jcp/146/18
Published by the American Institute of Physics